



Survey Accuracy Analysis of a Hand-held Mobile LiDAR Device for Cultural Heritage Documentation

TING ON CHAN, DEREK D. LICHTI, Calgary, Canada, DAVID BELTON, BERNHARD KLINGSEISEN & PETRA HELMHOLZ, Perth, Australia

Keywords: Zebedee, LiDAR, accuracy, fitting, geometric features

Summary: In this paper, the survey accuracy of a hand-held, GNSS-free mobile LiDAR device, the Zebedee, is studied by collecting measurements of several different geometric features in four different datasets. We use a new comprehensive accuracy assessment methodology based on geometric modelling which involves a geometric model of a prism/pyramid for square structure. The point cloud accuracies of the features (planes, cylinders, catenaries, prisms and pyramids) were compared to that of a conventional survey-grade LiDAR system, the Leica ScanStation C10. The results suggested that the Zebedee accuracy is very comparable to the C10. For instance, the mean RMS error of plane fittings for the Zebedee is approximately 1.1 cm versus 0.6 cm for the C10. The estimated cylinder radii between the Zebedee and the C10 has only 1.4% difference in average, while the radii difference in prism/pyramid fitting is only 0.8%. As a result, the Zebedee LiDAR device is suitable for heritage mapping not only because it has high operation flexibility but also desired high accuracy.

Zusammenfassung: *Genauigkeitsanalyse eines tragbaren Laserscanners für die archäologische Dokumentation.* Diese Veröffentlichung untersucht die Vermessungsgenauigkeit des tragbaren und ohne GNSS operierenden Laserscanners Zebedee unter Verwendung von geometrischen Objekten in vier verschiedenen Datensätzen. Die umfassende Bewertung der Genauigkeit basiert auf geometrischen Objekten, welche in der Punktwolke modelliert werden und Ebenen, Zylinder, gekrümmte Oberflächen, Prismen und Pyramiden einschließen. Die geometrischen Objekte werden mit Objekten verglichen, welche basierend auf Punktwolken von einem konventionellen vermessungsüblichen LiDAR System, der Leica ScanStation C10, modelliert wurden. Die Resultate zeigen, dass die Genauigkeit des Zebedee mit der des C10 vergleichbar ist. Zum Beispiel beträgt die kleinste Verbesserung für Ebenen (RMS) 1,1 cm gegenüber 0,6 cm vom C10. Die geschätzten Zylinderradien unterscheiden sich zwischen dem Zebedee und dem C10 im Durchschnitt nur um 1,4%. Der kleinste Radiusunterschied beim Prisma-/Pyramidenvergleich beträgt nur 0,8%. Daraus ist zu schließen, dass der Zebedee Laserscanner für die Dokumentation von denkmalgeschützten Gebäuden und Objekten geeignet ist, nicht nur basierend auf der höchst flexiblen Art der Anwendung, sondern auch von der Genauigkeitsbetrachtung her.

1 Introduction

Terrestrial mobile light detection and ranging (LiDAR) systems can be used to collect large point cloud datasets along with trajectories of the system (KUKKO et al. 2012). Conventionally, the point clouds collected by the systems at every epoch are directly geo-referenced to a local mapping frame by using the spatial information obtained from the integration of a

global navigation satellite system (GNSS) and an inertial navigation system (INS). In order to perform mobile mapping when GNSS signals are not available, or in harsh environments, GNSS-free scanning systems based on the principle of simultaneous localization and mapping (SLAM; CHOW et al. 2014) were introduced in recent years, e.g. BOSSE et al. (2012), ALISMAIL et al. (2014), VOSSELMAN (2014), ZHANG & SINGH (2014). Such systems

are particularly useful for cultural heritage or archaeological documentation since they are independent of the GNSS signals and also mostly compact and light, so users can carry the system to scan areas inaccessible to large vehicles. However, other than the manufacturers' own reports for such systems, very few research papers, e.g. THOMSON et al. (2013), focus on the evaluation of the resultant point cloud accuracy or the associated evaluation methods even though this is indeed often important for cultural heritage documentation. For instance, the captured point clouds often have to meet certain accuracy requirements that, depending on the type of object, can range from 5 mm to several centimetres. Where built structures with detailed ornamental features or surface textures are to be recorded, sub-centimetre accuracies are required. For features with a natural surface such as caves or stone walls, where it is important to record the overall dimensions rather than fine details, accuracies of up to 3 cm may be acceptable. In this paper, the point cloud accuracy of a hand-held spring-mounted mobile LiDAR system, the Zebedee (BOSSE et al. 2012, BOSSE & ZLOT 2013) is assessed by a geometric modelling methodology. Rather than primarily using plane fitting accuracy as an indicator to evaluate the Zebedee system (THOMSON et al. 2013), this work provides a more comprehensive study of the scanning accuracy through evaluating the fitting accuracy of geometric models of several common primitives including planes, cylinders, catenaries, and square prisms/pyramids. Using different geometric primitives for accuracy evaluation is advantageous over using artificial target points for several reasons: (1) higher data redundancy is obtained; (2) point intensity is not needed; (3) less labour cost is involved; (4) in situ accuracy evaluation is allowed. The accuracy obtained for the same features captured by a static terrestrial LiDAR is used as the reference. The accuracy of the Zebedee is studied as the device has been widely used for cultural heritage documentation (CSIRO 2015); it was used to scan the Leaning Tower of Pisa in Italy (ENGINEERING & TECHNOLOGY 2013) and various caves in Australia (ZLOT & BOSSE 2014).

The paper is organized as follows. First, the design and working principle of the Zebedee

are discussed in section 2, followed by the geometric models and methods used for assessing the accuracy in section 3. The experimental datasets are introduced in section 4. The paper concludes with the results and analysis in section 5.

2 Zebedee Scanner

The Zebedee was originally developed by the Autonomous Systems Laboratory at the Commonwealth Scientific and Industrial Research Organisation (CSIRO), based in Brisbane, Australia. It consists of a 2D scanner (Hokuyo UTM-30LX, horizontal field of view = 270° , maximum range = 30 m) mounted on a spring attached to a handle (Fig. 1). Scans are continuously captured with a swinging scanner head while the user is walking at a gentle speed. The user holds the handle and allows the scanner to swing back and forth along the walking direction (Fig. 2). An inertial measurement unit (IMU), MicroStation 3DM-GX2, is used to provide measurements of the scanner head motion at the initial stage and also during the scanning mission. A small laptop is integrated with the system for recording the data and is placed in a backpack.

The working principle of the Zebedee is based on SLAM in which the system trajectory is reconstructed by continuously estimating the six-degree-of-freedom (6-DOF) of the



Fig. 1: Zebedee scanner and its associated hardware.



Fig. 2: Scanner head's and the user's motion.

motion of the scanner head. This is done using the iterative closest point (ICP) method with input of surface patches identified from the scene. The 6-DOF between two subsequent epochs are estimated by the ICP which minimizes the distances between the conjugate surfaces patches, and also the deviation of IMU accelerations and rotation velocities (BOSSE et al. 2012).

3 Methodology

3.1 Reference Data

In order to analyse the accuracy of the Zebedee, a set of objects of interest in cultural heritage recording was captured with a Leica ScanStation C10. The C10 data were collected from different stations ensuring that all sides of the objects of interest were visible from at least one scan setup. Several Leica High Definition Surveying (HDS) targets were placed in the field of view of the scanner that allowed the registration of the individual point clouds into a common system, which was refined using the ICP method embedded in the Leica Cyclone.

3.2 Object Modelling

The fitting accuracy of several common geometric features was used in the comparison and analysis, with primary focus on simple geometric primitives such as planes, cylinders, catenaries and square prisms/pyramids. The geometric model used for fitting the planar and cylindrical features into the point cloud can be found in CHAN et al. (2015), and the geometric model of the 3D catenary curve in CHAN et al. (2013). Instead of setting up a target field for evaluation, a square building itself can be used by modelling all four facades simultaneously as a square prism or pyramid. The geometric models for a square prism/pyramid are derived from the octagonal pyramid model (CHAN & LICHTI 2014). The fundamental concept is to express one side of the square (in the first quadrant, red in Fig. 3a) with a tangent function with argument equal to half of the interior angle (90° for square). Thanks to its symmetry, all other sides of the prism are easily represented by rotation around the Z-axis. The model is given by (1) and (2), with the number of sides set as $n = 4$ and the gradient factor $k = 0$ for a square prism; and with $n = 4, k \neq 0$ for a square pyramid.

$$f(\bar{x}, \bar{l}) = [(R_0 - kZ') - X'] \tan\left(\left(1 - \frac{2}{n}\right) \cdot 90^\circ\right) - Y' = 0 \quad (1)$$

where

$$\begin{pmatrix} X' \\ Y' \\ Z' \end{pmatrix} = \mathbf{R}_3 \left((q-1) \cdot \frac{360^\circ}{n} + \Psi \right) \mathbf{R}_2(\Phi) \mathbf{R}_1(\Omega) \begin{pmatrix} X - X_c \\ Y - Y_c \\ Z \end{pmatrix} \quad (2)$$

and (X_c, Y_c) is the prism/pyramid centre in the XY -plane; Ω , Φ and Ψ are the rotation angles for the rotation matrices \mathbf{R}_1 , \mathbf{R}_2 and \mathbf{R}_3 about the X -axis, Y -axis and Z -axis, respectively. The rotational and translational parameters are depicted in Fig. 3b. The tetragonal radius (R_0) is defined at $Z = 0$, and q is defined as the quadrant number for each point with

$$q = \left\lceil \frac{\Theta n}{360^\circ} \right\rceil \quad (3)$$

where Θ ($0^\circ < \Theta \leq 360^\circ$) is the angle from the X -axis on the XY -plane in the normal position. q is calculated and updated during the fitting adjustment process and no pre-calculation is needed. The implementation of the fitting is based on the Gauss-Helmert adjustment model (FÖRSTNER & WROBEL 2004).

The quadrant number obtained from the fitting can be used to segment individual facades (planes) from the square prism/pyramid. The angle between two facades, θ , can be calculated by (4) and is used for the accuracy assessment

$$\theta = \cos^{-1} \left(\frac{|\bar{p}_1 \cdot \bar{p}_2|}{|\bar{p}_1| |\bar{p}_2|} \right) \quad (4)$$

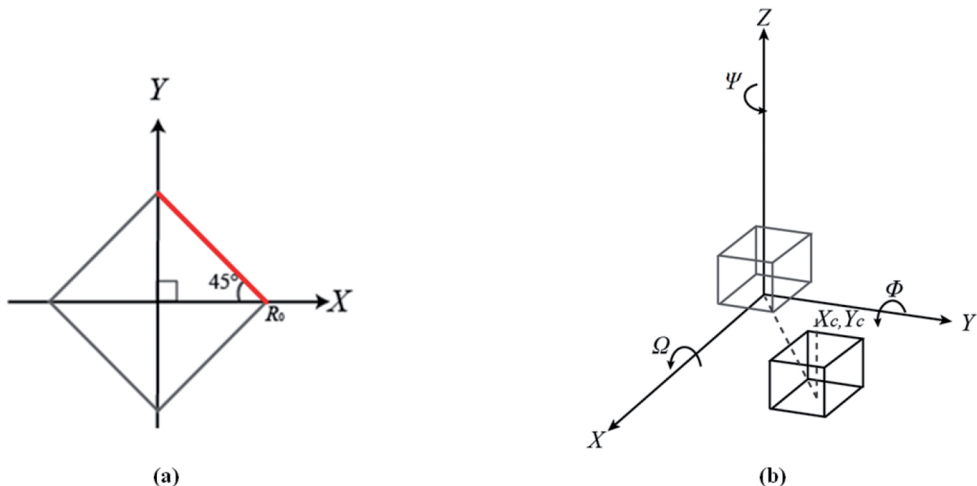


Fig. 3: Model parameters: (a) R_0 at the nominal position and (b) rotational and translational parameters.

where “ \bar{p}_1 Vektor” and “ \bar{p}_2 Vektor” are the direction cosine vectors for the two facades obtained from the fitting.

4 Experiments

Four datasets (1 – 4) were collected from several locations in Western Australia (WA), all located in the Murchison Region. The objects of interest in each dataset contain different dominant features such as planes, cylinders, catenaries, prisms, and pyramids, so the sites are very suitable to assess different aspects of the accuracy of the Zebedee scanner.

Dataset 1 (Fig. 4a) was collected using only the Zebedee. An artificial plane (a 60 cm \times 90 cm white flat board with 1 cm thickness mounted on a larger wooden board) was set in a vegetation rich area and scanned multiple times over a distance ranging from 1 m – 10 m, with an approximate interval of 0.5 m between scans. Only the white board was extracted based on its known dimension for the accuracy evaluation. The test was set out to determine if the accuracy of the trajectory reconstruction of the Zebedee depends on the variety of the object geometry in the field of

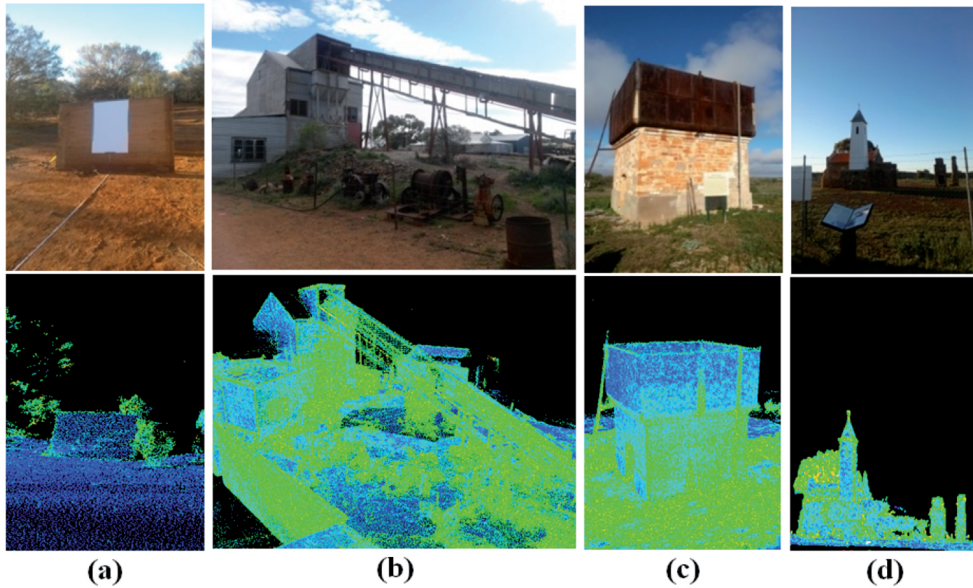


Fig. 4: Scenes and the Zebedee point clouds. (a) Dataset 1: an artificial plane with vegetation around (b) Dataset 2: gold battery (c) Dataset 3: water tank (d) Dataset 4: chapel.

view of the scanner. For all remaining datasets, the objects were captured using the Zebedee and the C10. Dataset 2 (Fig. 4b) was taken at the historical gold battery at Payne’s Find. This dataset contains cylindrical and catenary features such as circular oil tanks and power cables. Eight vertical and two horizontal cylinders, as well as three catenaries were extracted from Dataset 2. Dataset 3 (Fig. 4c) is a square water tank within the Yalgoo Railway Station Precinct. The stone masonry base was suitable for fitting a prism model. Dataset 4 (Fig. 4d) is the former Dominican Convent Chapel of St Hyacinth in Yalgoo. This dataset contains a 5 m tall square pyramid tower.

The first test focused on the plane fitting accuracy as a function of the distance of the Zebedee scanner to a plane. For this test the

ground surface was removed from the dataset for more effective histogram analysis. The normal vector and curvature information of the point cloud were computed using the CloudCompare software package v.2.6.1 for analysis. The implementation is based on the point cloud library (PCL; PCL 2015). Tests 2 – 4 required the detection and extraction of planes and the cylinders. This was done using a semi-automatic approach applying the random sample consensus (RANSAC) shape detection algorithm (SCHNABEL et al. 2007). This function was implemented as a plugin of the CloudCompare software package v.2.6.1. The catenaries were extracted manually using the same software. Some of the point clouds are shown in Fig. 5. A summary of the tests and used datasets is given in Tab. 1.

Tab. 1: Overview of the accuracy tests and the used data.

	Scans captured with		Dataset			
	Zebedee	C10	1	2	3	4
Accuracy tests						
1. Plane Fitting vs. Distance	×		×			
2. Cylinder and Catenary Fitting	×	×		×		
3. Square Prism Fitting	×	×			×	
4. Square Pyramid Fitting	×	×				×

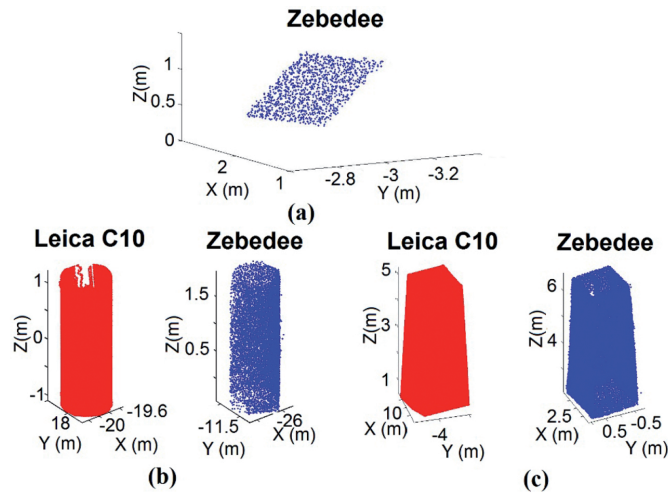


Fig. 5: Extracted point clouds: (a) Dataset 1: plane at 1 m, (b) Dataset 2: vertical cylinder, (c) Dataset 4: square pyramid.

5 Results and Analyses

5.1 Plane Fitting Accuracy of the Zebedee Vs. Distance (Dataset 1)

The root-mean-square (RMS) errors of the plane fitting versus the scanning distance are plotted in Fig. 6. The plane fit precision decreases from 1 m to 2 m scanning distance, and then gradually improves over the distance of 2 m–10 m. Although this behaviour is counter-intuitive since LiDAR precision generally degrades as a function of distance, it can be explained with reference to the operational principles of the Zebedee system. As the scanning distance increased, more of the surrounding environment, including vegetation, was scanned by the LiDAR system. Therefore, both the number of measured points and the geometric variety (as indicated by the increasing curvature statistics in Tab. 2 increased). Both factors improve ICP estimation that reconstructs the system trajectory. Accordingly, the plane measurement quality, i.e. lower RMS, was improved when more vegetation was scanned. The mean curvature is the average of the principal curvatures which is a quantity measuring how large a small surface (in a spherical neighbourhood having a radius of 2.5 cm) bends relatively to the tangent and normal planes defined by the surface nor-

mal. Therefore, point clouds with higher mean curvature exhibit greater geometric variation. The Zebedee developer performed a scanning test (BOSSE et al. 2012) on different environments containing different types of surfaces, e.g. hallway, courtyard, and grassland, and also found that lack of surfaces with high geometric variation during the scanning leads to less reliable trajectory reconstruction.

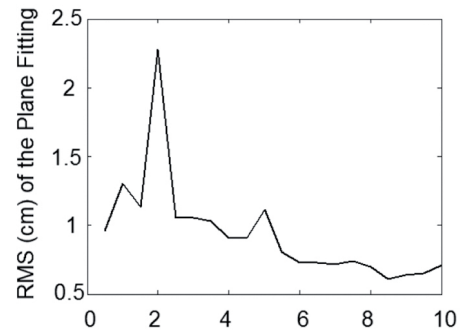


Fig. 6: RMS of plane fitting for the Zebedee point cloud versus scanning distance (top of each plot).

The mean RMS of the plane fitting for all the scanning distances is 9.4 mm, which represents approximately 30% of the mean error (32 mm) of the plane fitting reported in THOMSON et al. (2013). They compared the plane

fitting accuracy after registering the overall Zebedee point cloud with the referenced point cloud (captured by Faro Focus^{3D}). This additional step may have degraded the results. In addition, their Zebedee scans were performed inside an indoor rectangular walking corridor where vertical walls and floors/ceilings are the main reference objects for the trajectory reconstruction. The geometric variation in this environment, which is lower than that of the scene studied herein, may also be a reason for the lower accuracy.

The histograms of the planar residuals (distances between points-to-the best fit plane) for scanning distances 1 to 10 m are shown in Fig. 7. It can be seen that all the histograms at all scanning distances except at 2 m are approximately Gaussian in shape, so the planar model is appropriate. At 2 m, the residuals are not Gaussian (Fig. 7), and large residuals are randomly distributed (Fig. 8a) as the scanner positions are not accurately reconstructed due to lack of scans with high geometric variation which is indicated by the distribution of the

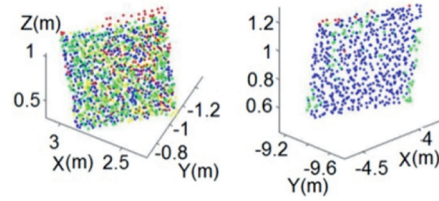


Fig. 8: Spatial distribution of the residuals of the plane fittings at (a) 2 m and (b) 10 m. Colour scale: blue = 0 cm – 1 cm, green = 1 cm – 2 cm, yellow = 2 cm – 3 cm, red > 3 cm.

curvature. Tab. 2 shows that the standard deviation at 2 m is the lowest while the mean of the fitted Gaussian of the curvature increases with the distances. The lowest standard deviation (σ) at 2 m implies the curvatures are the most homogenous so the scanner position cannot be accurately determined based on the SLAM. The mean of the fitted Gaussian increases with the scanning distance because in general more vegetation is scanned as the scanning distance increases.

Tab. 2: Statistics of the mean curvature histograms of the Zebedee point cloud (full scene) for Dataset 1. The mean curvature indicates the extent of the point cloud geometric variation.

Plane Scanning Distance (m)	No. of Points	Mean of Fitted Gaussian Distribution for the Curvature Histogram (m^{-1})	σ of the Fitted Gaussian Distribution for the Curvature Histogram (m^{-1})
1	184,870	0.1122	0.0646
2	192,550	0.1137	0.0627
4	216,232	0.1110	0.0677
7	240,968	0.1340	0.0788
10	361,289	0.1589	0.0840

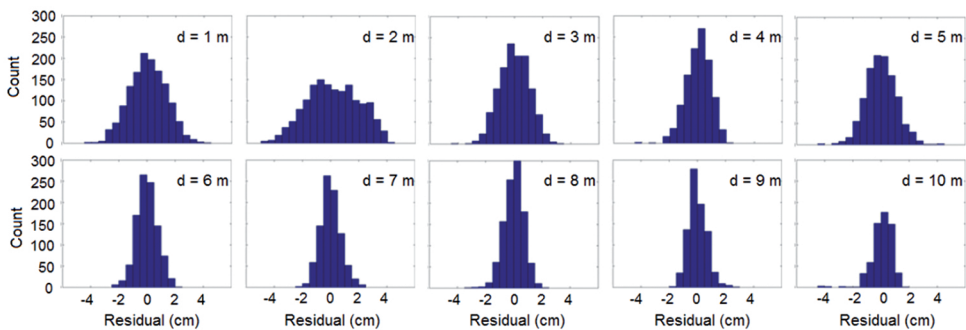


Fig. 7: Histograms of residual of the plane fittings at scanning distance (d) from 1 m to 10 m.

5.2 Geometric Fitting Accuracy

5.2.1 Cylinder and Catenary Fitting Accuracy (Dataset 2)

The RMS of the fitting residuals and the radii of the ten cylindrical objects scanned using both instruments are given in Tab. 3. While there is a significant difference in the RMS of the fitting between instruments partially due to the large differences in number of the observed points, the estimated radii are quite comparable. The smallest difference for the estimated radii is only 1 mm (Cylinder 4), while the mean relative difference of all radii is 1.4 %. The mean RMS error of the cylinder fitting for the C10 is approximately 5 mm while for the Zebedee it is 14 mm, so there is only approximately 8 mm difference. The F-test was carried for the cylinder fittings in which the empirical variances of the datasets are compared by computing the F-statistics. The F-tests are two tailed with 5% significance level, and the null hypothesis is $\sigma_{C10}^2 = \sigma_{ZEB}^2$. Only two out of the ten cylinder fittings has the null hypothesis which are not rejected, so the difference between two sets of fitting are statistically significant even though

the differences between the estimated radii of the two datasets for most of the fittings are on millimetre level.

The overall accuracy of cable-like objects modelled as catenary curves is lower (Tab. 4). Since the cable-like objects are very thin, the reflected laser energy was diminished due to the expanding beam width. The fitting accuracy of the Zebedee is approximately 24 mm lower than the one using the C10. The spatial distribution of the residuals for some of the features for C10 and Zebedee are shown in Figs. 9 – 11. It can be seen that the Zebedee form-fitting errors are randomly distributed. The majority of the errors fall in the range 0 cm – 1 cm. The Zebedee accuracy for catenary is not as high as for cylinder compared to the C10 but it can still be used for catenary survey if centimetre level of accuracy is desired.

Tab. 4: RMS of the catenary curve fitting.

RMS of the Catenary Fitting (m)		
Catenary	Leica C10	Zebedee
1	0.018	0.052
2	0.008	0.027
3	0.016	0.037
Mean	0.014	0.039

Tab. 3: RMS and estimated radii of the cylinder fitting (Cylinders 1 – 8 are vertical; Cylinders 9 – 10 are horizontal).

Cylinder	No. of points (Approx. scanning distance (m))		RMS of the fitting residuals		Estimated Radius, r		
	Leica C10	Zebedee	Leica C10 (m)	Zebedee (m)	Leica C10 (m)	Zebedee (m)	Difference (%)
1	88,608 (4)	8,753 (2)	0.003	0.012	0.383	0.371	2.9
2	16,418 (5)	2,725 (2)	0.005	0.017	0.288	0.290	0.5
3	263,159 (5)	6,980 (2)	0.006	0.011	1.272	1.279	0.6
4	23,386 (2)	2,499 (2)	0.007	0.015	0.253	0.254	0.4
5	5,688 (6)	610 (3)	0.004	0.015	0.287	0.278	3.2
6	2,415 (7)	441 (3)	0.005	0.014	0.281	0.276	1.8
7	8,103 (5)	1,406 (2)	0.006	0.015	0.289	0.293	1.3
8	9,694 (5)	1,188 (2)	0.005	0.012	0.287	0.285	0.8
9	8,327 (5)	1,055 (2)	0.002	0.009	0.255	0.261	2.5
10	6,619 (6)	374 (5)	0.008	0.021	0.378	0.376	0.5
Mean			0.005	0.014			

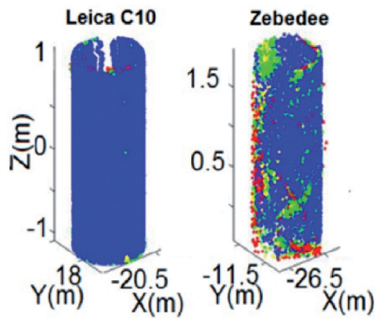


Fig. 9: Spatial distribution of the residuals (point-to-model distances) for Cylinder 1 (Vertical). Colour scale: blue = 0 cm – 1 cm, green = 1 cm – 2 cm, yellow = 2 cm – 3 cm, red > 3 cm.

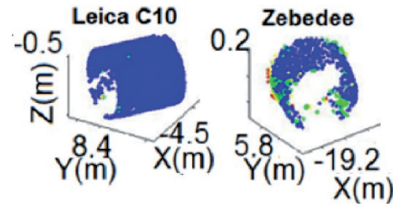


Fig. 10: Spatial distribution of the residuals (point-to-model distances) for Cylinder 9 (Horizontal). Colour scale: blue = 0 cm – 1 cm, green = 1 cm – 2 cm, yellow = 2 cm – 3 cm, red > 3 cm.

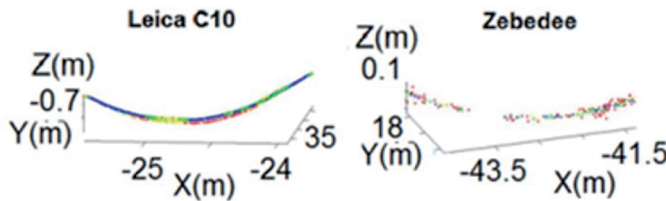


Fig. 11: Spatial distribution of the residuals (point-to-model distances) for Catenary 1. Colour scale: blue = 0 cm – 1 cm, green = 1 cm – 2 cm, yellow = 2 cm – 3 cm, red > 3 cm.

5.2.2 Square Prism Fitting Accuracy (Dataset 3)

Tab. 5 shows the RMS and the estimated radius (R_0) of the stone masonry base of the water tank obtained from fitting the square prism model ((1) and (2)). The residual statistics differ less than 7 mm and the estimated radii only differ by 0.8%. Tab. 6 shows the residuals for individual planes according to quadrant number (as each point is associated with a unique quadrant number) after the square prism fitting. The results are consistent with those of test 2 (cylinder fitting). The angles computed between adjacent walls are shown in Tab. 7. All angles of the square prism are close to 90° . The similarity of the derived angles suggests that the measurement accuracy of the Zebedee is comparable to that of the C10. However, Fig. 12 shows that one wall has a greater number of errors in the 1 cm – 2 cm range and errors > 3 cm concentrated near the edges. This lower accuracy of the wall measurement is likely attributed to relatively higher swinging/moving speed of the scanner (this condition is

unique for Dataset 3). This indicates that the motion stability of the system is also a factor of the limited accuracy (KAUL et al. 2015), but would require further investigation to confirm. The results also suggest that the Zebedee tends to have lower accuracy at wall edges probably due to the edge effect (only relatively smaller part of laser energy is reflected at edges compared to flatter surfaces), but again further study is needed.

5.2.3 Square Pyramid Fitting Accuracy (Dataset 4)

The height of the extracted square pyramid of the Chapel tower is approximately 5 m. The estimated radii and gradient factor (position/orientation-independent parameters) between the Zebedee and the C10 tower differ by about 7% (Tab. 8). This discrepancy is much higher than the results in the previous test (note that k was not estimated for the previous test of the square prism). Since the tower was scanned the same way as the water tank in the previous test (the operator held the scanner and

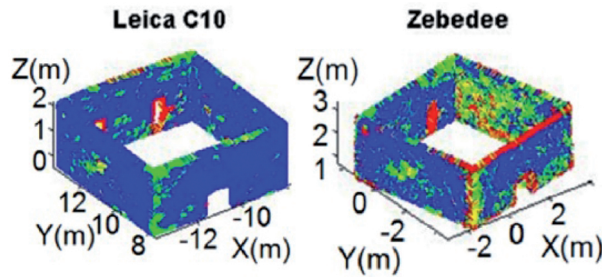


Fig. 12: Spatial distribution of the prism residuals (point-to-model distances). Colour scale: blue = 0 cm – 1 cm, green = 1 cm – 2 cm, yellow = 2 cm – 3 cm, red > 3 cm.

Tab. 5: RMS and estimated radii of the square prism fitting for Dataset 3.

	RMS	Estimated R_0			
	Leica C10 (m)	Zebedee (m)	Leica C10 (m)	Zebedee (m)	Diff. (%)
Water Tank	0.007	0.014	4.088	4.120	0.8

walked around the target in an open field), the reference objects for the ICP estimation were only the target itself and some sparse vegetation in both tests. Under similar scanning reference conditions, the scanning range of the tower (approximately 5 m – 8 m) is higher than that of the previous test (approximately 2 cm – 3 m). As a result, the measurement accuracy of the tower is lower. In addition, the scanning orientation was significantly different compared to the previous test because the object was 1 m – 5 m above the scanner. So, there are no horizontal reference objects available at the same height. Even though the estimated model parameters for the prism/pyramid differed more, the plane fitting accuracies for the individual parts were consistent with previous test results (Tab. 9). However, the deviations between interior angles are slightly higher compared to previous tests (Tab. 10). This is likely due to the fact that the walls are much shorter in this case. The mean side length of the tower and the water tank are 0.95 m and 5.76 m, respectively. Therefore, errors in the perpendicular distances (Zebedee) for the tower and water tank corresponding to mean angular errors, 0.328° and 0.267° , are 5.43 mm and 2.68 mm, respectively. Fig. 13 shows that

many points with the larger errors are distributed near the top for both the scanners and near the edges (similar to the water tank) in the Zebedee point cloud.

6 Conclusion

In this paper, the survey accuracy of the Zebedee scanner, a SLAM-based hand-held mobile mapping LiDAR device, was intensively studied. The accuracy was accessed using multiple types of geometric primitives with their models fitting to point clouds of objects at several cultural heritage sites in Australia. The primitive-based accuracy evaluation method has several merits over the point-based method for several reasons such as higher redundancy can be obtained and point intensity is not needed. The fitting accuracy was compared to that of a conventional high accuracy terrestrial LiDAR scanner, the Leica ScanStation C10. The results suggest that the availability and geometric variation of the surrounding reference objects are important for capturing more accurate Zebedee point cloud. For feature measurement, the Zebedee accuracy is very comparable to the C10, with centimetre-level dif-

Tab. 6: RMS of plane fitting.

	RMS of the Plane Fitting (m)	
	Leica C10	Zebedee
Wall 1	0.010	0.013
Wall 2	0.006	0.010
Wall 3	0.005	0.013
Wall 4	0.005	0.014
Mean	0.007	0.013

Tab. 7: Estimated angles between two walls for Dataset 3.

	Angle between two walls (°)	
	Leica C10	Zebedee
Wall 1 & 2	89.889	89.965
Wall 2 & 3	89.850	89.981
Wall 3 & 4	89.928	89.958
Wall 1 & 4	89.889	89.989

Tab. 8: RMS and estimated parameters of the square pyramid fitting for Dataset 4.

	RMS		Estimated R_0			Estimated k		
	Leica C10 (m)	Zebedee (m)	Leica C10 (m)	Zebedee (m)	Diff. (%)	Leica C10	Zebedee	Diff. (%)
Tower	0.007	0.012	1.178	1.257	6.7	0.0562	0.0522	7.1

Tab. 9: RMS of plane fitting.

	RMS of the Plane Fitting (m)	
	Leica C10	Zebedee
Wall 1	0.006	0.013
Wall 2	0.006	0.009
Wall 3	0.005	0.011
Wall 4	0.005	0.010
Mean	0.006	0.011

Tab. 10: Estimated angles between two walls for Dataset 4.

	Angle between two walls (°)	
	Leica C10	Zebedee
Wall 1 & 2	89.937	89.591
Wall 2 & 3	89.636	90.094
Wall 3 & 4	89.936	89.611
Wall 1 & 4	90.594	90.420

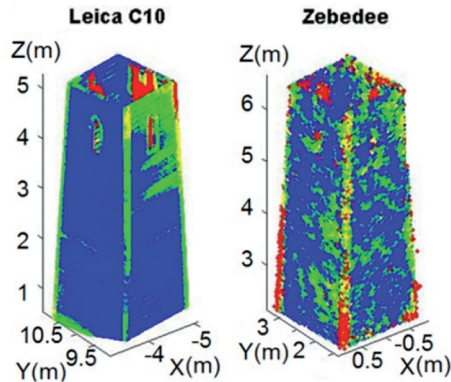


Fig. 13: Spatial distribution of the pyramid residuals (point-to-model distances). Colour scale: blue = 0 cm – 1 cm, green = 1 cm – 2 cm, yellow = 2 cm – 3 cm, red > 3 cm.

ferences in plane fitting. The mean RMS errors for plane, cylinder, catenary, prism and pyramid fitting for the Zebedee point clouds were all less than 1.5 cm. The estimated cylinder radii between the Zebedee and the C10 differed by only 1.4% difference on average, while the radii difference from the prism/pyramid fitting was 0.8%. Overall, the Zebedee scanner is suitable for heritage mapping, not only because of its ease of use (extensive training for the operation and data processing are not needed), but also because the desired centimetre-level accuracies can be achieved. In addition, due to its portability and compactness, the Zebedee can be operated in areas that may be inaccessible for conventional terrestrial scanners.

Acknowledgement

This research was partially supported by an Australian Endeavour Research Fellowship (2014) awarded to the first author by the Australian Government. The data were collected during the site survey for the Curtin University Survey Expedition 2014 sponsored by the following organizations: RM Surveys, Whelans, Land Surveys, Cottage & Engineering Surveys, McMullen Nolan Group, Silver Lake Resources, C.R. Kennedy, Haefeli-Lynar, Landgate, State Heritage Office, SSSI, LSLB and WAIS. We want to thank CSIRO

for providing the Zebedee for this research project and the associated training. The authors would also like to thank all the staff, volunteers and students who participated in the Survey Expedition.

References

- ALISMAIL, H., BAKER, D. & BROWNING, B., 2014: Continuous trajectory estimation for 3D SLAM from Actuated LiDAR. – IEEE International Conference on Robotics & Automation (ICRA), Hong Kong, China.
- BOSSE, M., ZLOT, R. & FLICK, P., 2012: Zebedee: Design of a spring-mounted 3-D range sensor with application to mobile Mapping. – IEEE Transactions on Robotics **28** (5): 1–15.
- BOSSE, M. & ZLOT, R., 2013: Place recognition using keypoint voting in large 3D Lidar datasets. – IEEE International Conference on Robotics and Automation, Karlsruhe, Germany.
- CHAN, T.O., LICHTI, D.D. & GLENNIE, C., 2013: Multi-Feature based boresight self-calibration of a terrestrial mobile mapping system. – ISPRS Journal of Photogrammetry and Remote Sensing **82**: 112–124.
- CHAN, T.O. & LICHTI, D.D., 2014: Geometric modeling of octagonal lamp poles. – International Archives of Photogrammetry, Remote Sensing and Spatial Information Sciences XL-5, ISPRS Technical Commission V Symposium, Riva del Garda, Italy.
- CHAN, T.O., LICHTI, D.D. & BELTON, D., 2015: A rigorous cylinder-based self-calibration approach

- for terrestrial laser scanners. – *ISPRS Journal of Photogrammetry and Remote Sensing* **99**: 84–99.
- CHOW, J.C., LICHTI, D.D., HOL, J.D., BELLUSCI, G. & LUINGE, H., 2014: IMU and multiple RGB-D camera fusion for assisting indoor stop-and-go 3D terrestrial laser scanning. – *Robotics* **3**: 247–280.
- CSIRO, 2015: Zebedee. – <https://wiki.csiro.au/display/ASL/Zebedee> (17.8.2015).
- ENGINEERING & TECHNOLOGY, 2013: Spring-mounted Zebedee maps Pisa Tower in 3D. – <http://ieeexplore.ieee.org/stamp/stamp.jsp?arnumber=6676302> (17.8.2015).
- FÖRSTNER, W. & WROBEL, B., 2004: Mathematical concepts in photogrammetry. – McGLONE, J.C., MIKHAIL, E.M., BETHEL, J. & MULLEN, R. (eds.): *Manual of Photogrammetry*: 15–180, 5th ed., ASPRS, Bethesda, MD, USA.
- KAUL, L., ZLOT, R. & BOSSE, M., 2015: Continuous-time three-dimensional mapping for micro aerial vehicles with a passively actuated rotating laser scanner. – *Journal of Field Robotics*: 1–30.
- KUKKO, A., KAARTINEN, H., HYYPPÄ, J. & CHEN, Y., 2012: Multiplatform mobile laser scanning: usability and performance. – *Sensors* **12** (9): 11712–11733.
- PCL, 2015: Estimating surface normals in a point cloud. – Point Cloud Library; http://pointclouds.org/documentation/tutorials/normal_estimation.php (20.8.2015).
- SCHNABEL, R., WAHL, R. & KLEIN, R., 2007: Efficient RANSAC for point-cloud shape detection. – *Computer Graphics Forum* **26** (2): 214–226.
- THOMSON, C., APOSTOLOPOULOS, G., BACKES, D. & BOEHM, J., 2013: Mobile laser scanning for indoor modelling. – *ISPRS Annals of Photogrammetry, Remote Sensing and Spatial Information Sciences II (5/W2)*, ISPRS Laserscanning Workshop, Antalya, Turkey.
- VOSSELMAN, 2014: Design of an indoor mapping system using three 2D laser scanners and 6 DOF SLAM. – *ISPRS Annals of the Photogrammetry, Remote Sensing and Spatial Information Sciences, II(3)*, ISPRS Technical Commission III Symposium, Zurich, Switzerland.
- ZHANG, J. & SINGH, S., 2014: LOAM: Lidar odometry and mapping in real-time. – *Robotics, Science and Systems Conference*, Berkeley, CA, USA.
- ZLOT, R. & BOSSE, M., 2014: Three-dimensional mobile mapping of caves. – *Journal of Cave and Karst Studies* **76** (3): 191–206.

Addresses of the Authors:

Ph.D. TING ON CHAN & Prof. Ph.D. DEREK D. LICHTI, Department of Geomatics Engineering, Schulich School of Engineering, University of Calgary, 2500 University Dr NW, Calgary, Alberta, T2N1N4 Canada, Tel.: {+1-403-210-7140}{+1-403-210-9495}, Fax: +1-403-284-1980, e-mail: {ting.chan} {ddlichti} @ucalgary.ca

Ph.D. DAVID BELTON, Department of Spatial Sciences, Curtin University, GPO Box U1987, Perth, WA 6845, Australia, Tel.: +61-8-9266-2704, Fax: +61-8-9266-2703, e-mail: d.belton@curtin.edu.au

Dr. DI (FH). BERNHARD KLINGSEISEN, State Heritage Office, Bairds Building, Level 2, 491 Wellington Street, Perth WA 6000, Australia, Tel.: +61-8-6552-4060, Fax: +61-8-6552-4001, e-mail: bernhard.klingseisen@stateheritage.wa.gov.au

Dr.-Ing. PETRA HELMHOLZ, Department of Spatial Sciences, Curtin University, GPO Box U1987, Perth, WA 6845, Australia, Tel.: +61-8-9266-3369, Fax: +61-8-9266-2703, e-mail: petra.helmholz@curtin.edu.au

Manuskript eingereicht: September 2015

Angenommen: April 2016